Lithosphere Destabilization by Melt Weakening and Crust-Mantle Interactions : Implications for Generation of Granite-Migmatite Belts

Kaislaniemi, L.

2018-09

Kaislaniemi , L , van Hunen , J & Bouilhol , P 2018 , ' Lithosphere Destabilization by Melt Weakening and Crust-Mantle Interactions : Implications for Generation of Granite-Migmatite Belts ' , Tectonics , vol. 37 , no. 9 , pp. 3102-3116 . https://doi.org/10.1029/2018TC005014

http://hdl.handle.net/10138/300149
https://doi.org/10.1029/2018TC005014

unspecified
publishedVersion

Tectonics

RESEARCH ARTICLE
10.1029/2018TC005014

Lithosphere Destabilization by Melt Weakening and Crust-Mantle Interactions: Implications for Generation of Granite-Migmatite Belts

L. Kaislaniemi[1,2], J. van Hunen[1], and Pierre Bouilhol[3]

[1]Department of Earth Sciences, Durham University, Durham, UK, [2]Department of Geosciences and Geography, University of Helsinki, Helsinki, Finland, [3]Université de Lorraine, Centre de Recherches Pétrographiques et Géochimiques, UMR7358, Vandœuvre-les-Nancy, France

Key Points:
- Partial lithosphere melting leads to positive feedback with convective lithosphere thinning
- Postcollisional lithosphere thermal relaxation initiates lower crustal anatexis
- Process explains temporal order of migmatites, granitic plutons, and intervening mantle melts

Correspondence to:
L. M. Kaislaniemi,
lars.kaislaniemi@iki.fi

Citation:
Kaislaniemi, L. M., van Hunen, J., & Bouilhol, P. (2018). Lithosphere destabilization by melt weakening and crust-mantle interactions: Implications for generation of granite-migmatite belts. *Tectonics*, *37*, 3102–3116. https://doi.org/10.1029/2018TC005014

Received 2 FEB 2018
Accepted 31 AUG 2018
Accepted article online 4 SEP 2018
Published online 19 SEP 2018

Abstract Orogenic crustal anatexis is a still poorly understood process due to the complexity of the thermal and geodynamical interaction between mantle and crustal processes during and after continental collision. Here we present a novel conceptual model for the formation of granite-migmatite belts: we propose that convective thinning of the lithosphere results in minor amounts of partial melts within the lowermost crust that trigger further instabilities. This will lead to positive feedback effects between melt weakening, mantle upwelling, and wholesale mantle lithosphere removal, causing a strong pulse of mantle and crustal melting. We test this model numerically, and results show that this process, taking between 20 and 50 Myr in total, can explain the temporal evolution of melting in granite-migmatite zones and associated mantle-derived mafic rocks and provides a heat source for crustal melting without the need for other processes, such as slab break-off or increased radiogenic heating. Furthermore, the generation of a refractory residue after mantle and crustal melting is also shown to control the progress of the lithospheric mantle removal, providing another feedback mechanism between melting and lithospheric reequilibration.

1. Introduction

Thickened orogenic crust is found to be or have been in a partially molten state in modern (Nelson et al., 1996; Schilling et al., 1997) and in past orogenies (Brown, 2001; Vanderhaeghe & Teyssier, 2001). Partial melting of the lower crust during the evolution of an orogen produces granite-migmatite belts that have been generally attributed to either (a) thickening of the crust during orogenesis and associated increase in the radiogenic heating raising the geotherm enough for crustal anatexis (Bea, 2012; Thompson & Connolly, 1995) or (b) a *thermal pulse* from the mantle, induced by slab break-off (Davies & von Blanckenburg, 1995) or convective thinning, delamination, or foundering of the thickened lithospheric mantle (Bonin, 2004; Platt & England, 1994; Sylvester, 1998; Yuen & Fleitout, 1985).

To reach high enough temperatures for anatexis by crustal thickening only, twice the original crustal thickness is needed (Bea, 2012; Thompson & Connolly, 1995). This mechanism is especially problematic in regions where syncollisional high-temperature/low-pressure metamorphism points to only modest crustal thickening (Finger et al., 2009; Franke, 2000). Therefore, a nonnegligible mantle contribution to the increased temperatures is often necessary to explain the formation of widespread crustal melting. This mantle contribution in the generation of the granite-migmatite belts is supported by the presence of primitive (ultra)potassic magmas, either as intrusive bodies or as a ubiquitous component of the granitoids (e.g., Couzinié et al., 2014, 2016; Ledru et al., 2001; Väisänen et al., 2000). Based on their geochemistry, the mantle-derived magmas are interpreted to originate from a hydrous metasomatic mantle (Bonin, 2004; Murphy, 2013; Turner et al., 1996), and their underplating at the crust-mantle transition zone (CMTZ; e.g., Williamson et al., 1992) would promote crustal melting through heat advection (Petford & Gallagher, 2001).

Cessation of the tectonic compression and a sudden change in the gravitational potential energy by foundering of the lithospheric mantle and subsequent dynamic uplift are thought to cause orogenic collapse at the later stages of the orogeny (Dewey, 1988). Collapse (synconvergent extension) is even possible with continuing tectonic convergence and compression, since crustal melting causes rheological weakening of the lower to middle crust (Gray & Pysklywec, 2012; Vanderhaeghe & Teyssier, 2001). The collapse induces crustal

extension as the upper crust is free to slide on top of the flowing midcrust (Bouilhol et al., 2006) and rapidly exhumes granite-migmatite zones, thus playing an important role in formation of gneiss domes and core complexes. Rapid exhumation might also enhance the melting as pressure decreases (Teyssier & Whitney, 2002).

A rheologically weak layer at or near the CMTZ has also been recognized as an important feature and a prerequisite for mantle delamination (Bird, 1979; Meissner & Mooney, 1998). Usually, this decoupling is thought to arise from the rheological layering of the lithosphere, where the lower crust is inherently weaker than the underlying lithospheric mantle, decoupling these two from each other, and allowing the negatively buoyant lithospheric mantle to sink into the asthenosphere. Even small melt fractions can significantly weaken crustal rocks (e.g., Rosenberg & Handy, 2005), suggesting that, if present near or at the CMTZ, partial melting could also cause such a weak layer, too.

Numerical and conceptual models of both crustal collapse (e.g., Jamieson et al., 2004; Liu & Yang, 2003; Rey et al., 2010; Teyssier & Whitney, 2002) and foundering of lithospheric mantle (e.g., Chung et al., 2003; Göğüş & Pysklywec, 2008; Göğüş et al., 2017; Nelson, 1992) are numerous, but the interaction of these two processes has gained less attention. In many models of crustal collapse the focus lies in the exhumation and extension of the crust, and thus, the lower boundary of the model is the lithosphere-asthenosphere boundary, which does not give the mantle convection an active role or allow for dynamic mass transfer between lithosphere and asthenosphere. With the exception of few (e.g., Ueda et al., 2012) models of lithospheric foundering, crustal processes do not possess an active and evolving role but are only passively responding to mantle processes, for example, melting, extension, and collapse after removal of the lithospheric mantle. Numerical models of other geological settings (e.g., Gerya & Meilick, 2011) that incorporate dynamic melting models have shown the importance of rheological weakening by fluids and melts to the overall dynamics of the system.

Widespread crustal anatexis in synorogenic to postorogenic processes, that is, formation of the granite-migmatite belts, is important not only for the crustal collapse and extension but also for the underlying mantle lithosphere dynamics: Melt-induced weakening in the lower crust could drive the crust-mantle decoupling even further and can trigger wholesale, *catastrophic* mantle lithosphere removal and thus strong asthenospheric upwelling. For example Göğüş and Pysklywec (2008) have shown that this would happen in the presence of an explicitly imposed weak layer. Here we propose and test a more dynamic hypothesis, in which partial melting and layer decoupling reinforce each other. For this purpose, we present numerical models of convectively thinning postcollisional lithosphere, integrated with melting models for both mantle and crustal melts, and melt-induced rheological weakening. We use these models to show that crustal and mantle processes interact in a fundamental way, where not only the processes taking place in the mantle affect generation of granite-migmatite belts but also the anatexis within the crust can change the evolution of the whole lithosphere.

2. Methods

We study the convection and melting of the mantle and crust in a syncollisional to postcollisional setting where the mantle rocks are overlain by a moderately thickened crust. Our models assume a metasomatic mantle which has been hydrated by a previous subduction system and where water is accommodated by both nominally anhydrous phases and hydrous phases. Water in nominally anhydrous mantle phases decreases their viscosity (e.g., Mei & Kohlstedt, 2000)—and consequently the upper mantle viscosity—enhances sublithospheric convection and leads to localized thinning of the mantle lithosphere. Melting in the crust and in the mantle is dynamically coupled to the convecting mantle, and feedback effects by consumption of latent heat and changes in the rock composition and physical parameters (viscosity and density) are taken into account.

2.1. Mantle Convection Model

We solve the equations for conservation of mass, momentum, and energy with a finite element code Citcom (Moresi & Gurnis, 1996; Zhong et al., 2000) to model the mantle convection in a 2-D model domain with dimensions of 660 km × 2,640 km and grid resolution of 64 × 256 elements. Adiabatic heating, shear heating, and heating by radioactive elements are taken into account (extended Boussinesq approximation; Christensen & Yuen, 1985). A linear temperature, pressure, and water content-dependent rheology is used, similar to the one

Table 1
Values of Physical Parameters Used in the Models

Parameter	Symbol (unit)	Value used
Activation energy	E (J/mol)	1.2×10^5
Activation volume	V (m^3/mol)	6×10^{-6}
Radiogenic heating	Q (W/kg)	19×10^{-12}
Thermal diffusivity	κ (m^2/s)	10^{-6}
Heat capacity	C_p ($J \cdot kg^{-1} \cdot K^{-1}$)	1, 250
Reference temperature	$T_{0,abs}$ (K)	1, 623
Reference pressure	P_0 (Pa)	21.4×10^9
Reference viscosity	η_0 (Pa s)	10^{22}
Effective visc. (min, max limit)	η (Pa s)	10^{17}, 10^{27}
Reference density	ρ_0 (kg/m^{-3})	3, 300
Latent heat of melting	L (J/kg^{-1})	5.6×10^5
Coefficient of thermal expansion	α (K^{-1})	3.5×10^{-5}

used by Kaislaniemi et al. (2014) but extended with a melt weakening parameterization:

$$\eta = \eta_0 \eta_\phi 100^{\frac{X_{H_2O}}{a+X_{H_2O}}} \exp\left(\frac{E+PV}{RT_{abs}}\right) \exp\left(-\frac{E+P_0V}{RT_{0,abs}}\right) \quad (1)$$

where η is the effective viscosity, η_ϕ melt weakening coefficient (see below), X_{H_2O} water content of the nominally anhydrous minerals in the mantle (ppmH_2O), and $a = 300$ppmH_2O a parameter controlling how large X_{H_2O} has to be to lower the viscosity by 1 order of magnitude (Kaislaniemi et al., 2014). See Table 1 and Figure 1 for other parameters and their values. Linear rheology with low thermal activation energy has been shown (van Hunen et al., 2005) to produce similar thermal boundary layer dynamics than a non-linear rheology ($n = 3.5$) with an activation energy in the range of 360 to 540 kJ/mol. We therefore use this parameterization instead of nonlinear rheology, which is numerically more challenging to solve.

Melt weakening of the rock, caused by unextracted partial melts occupying grain boundaries, is parameterized with a relation

$$\frac{\dot{\epsilon}(\phi)}{\dot{\epsilon}(0)} = \exp(\beta\phi) \quad (2)$$

(Mei et al., 2002), where $\dot{\epsilon}$ is the strain rate, ϕ is the melt fraction, and $\beta \approx 26$ in the diffusion creep regime. With a linear rheology, this converts to

$$\eta_\phi = \exp(-\beta\phi) \quad (3)$$

Melt weakening is limited by the forced lower limit for the viscosity (see Table 1).

For the lithospheric structure, we use the so called *jelly sandwich* rheology model (Burov & Watts, 2006) where the base of the crust is significantly weaker than the lithospheric mantle (Kohlstedt et al., 1995; Ranalli & Murphy, 1987; Wang et al., 2012). This provides a possible zone for the decoupling of crust and lithospheric mantle. The cause of this weak layer is the thermally activated creep of the wet quartz and feldspars below the brittle/ductile transition depth (Rybacki et al., 2006). The extent of this weakening, however, has been subject to debate (Jackson, 2002). We simplify the rheological model by using the same diffusion creep rheology for both the crust and the mantle and lowering the effective viscosity of the crust by 2 orders of magnitude. Together with the temperature-dependent viscosity this leads to an effective viscosity profile where there is a weak layer in the transition from mantle to lower crust but then at the shallower (i.e., cooler) depths the strength of the lithosphere quickly increases again.

A marker-in-cell method (Gerya & Yuen, 2003) is used to carry and advect temperature and lithological information. There are on average 40 markers per grid element, of which 50% carry the rock composition information for melting models, and all markers are used for temperature advection. Each marker represents a constant volume fraction of a grid element.

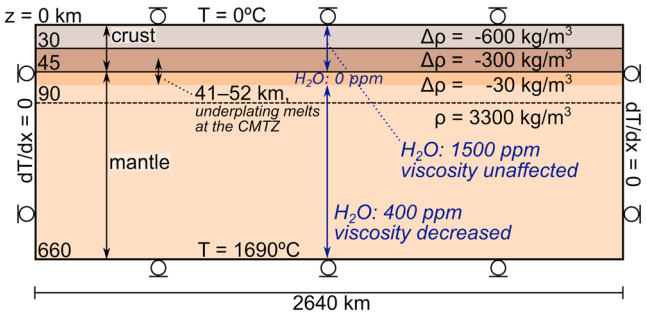

Figure 1. Model setup (not to scale). Brown/gray colors: crust; red colors: mantle. Mantle densities can vary dynamically according to equation (4). CMTZ = crust-mantle transition zone.

Table 2
Parameter Settings for the Presented Model Calculations

Model	Melt weakening	Mantle melt extraction	Crustal melt extraction
M000	Off	Off	Off
M100	On	Off	Off
M110	On	On	Off
M111	On	On	On

2.2. Melting Models

The models consider the melting of crustal and mantle rocks. For the mantle rocks, we use a parameterized melting model of hydrous peridotite by Katz et al. (2003). For crustal rocks, we calculate the liquidus and the amount of melt via a Gibbs free energy minimization strategy with PerpleX (Connolly, 2005; 2009). This permits a dynamic integration of the melting models so that the solidus of the crustal lithology depends on its fertility through its composition and melt depletion.

The parameterized melting model of the mantle rocks gives the amount of melt produced and the water content of the melt given the pressure, temperature, and water content of the bulk rock (a peridotite). This is used in the convection model to (1) modify the residual water content with bulk partitioning coefficient $D_{H_2O} = 0.01$ as used by Katz et al. (2003); (2) modify the rocks' effective mantle viscosity due to melt weakening and amount of water present, according to equation (1); (3) calculate the amount of latent heat consumed in the melting; and (4) modify the density of the residue. The density ρ of lherzolite reduces with depletion $F_{\%}$, following the relation

$$\frac{\mathrm{d}\ln\rho}{\mathrm{d}F_{\%}} = -0.00020 \tag{4}$$

which is applicable at approximately 3 GPa (Schutt & Lesher, 2006). Here $F_{\%} = 100F$, where F is the depletion parameter, that is, the fraction of total extracted melt from the bulk rock.

PerpleX performs Gibbs energy minimization for a given crustal rock composition, carried within the lithology information of the markers. Input parameters are the amounts of major elements (in this case in NCKFMASHT: Na_2O, CaO, K_2O, FeO_T, MgO, Al_2O_3, SiO_2, H_2O, and TiO_2), pressure, temperature, and the thermodynamic data libraries for the minerals and the solid solutions. We use the thermodynamic data from Holland and Powell (1998, revised in 2004), and their solid solutions (for garnet, pyroxenes, olivine, spinel, biotite, mica, chlorite, and chloritoid), except for amphibole (Wei & Powell, 2003; White et al., 2003), feldspars (Fuhrman & Lindsley, 1988), melt (White et al., 2001)—with modified pressure dependency of a sillimanite liquid from Bouilhol et al. (2015)—and the equation of state of water from Holland and Powell (1991). Results from the Gibbs energy minimization include the amount and composition of the stable phases (i.e., of minerals and liquid phases). This information is used (1) to modify the residue composition (all nine major oxides), which then affects subsequent melt processes, and (2) to calculate the consumption of latent heat in the melting. PerpleX results are tabulated prior to model run for unmodified rock compositions and recalculated each time step for modified rock compositions that are not available within the lookup table.

Depending on model parameters (Table 2), melts are extracted in some models and left in place in other models. Where melts are removed, the properties of the melt-depleted residue are updated with the information from the melting models, as described above. If melts are retained, the amount of melting is only recorded but the chemical properties of the bulk rock are not changed (i.e., the melt is assumed to stay in equilibrium with the rock and the latent heat of melting is still available for the rock during subsequent time steps).

Where crustal melts are extracted the melt (mass and latent heat) is removed from the model domain and its amount recorded. Where mantle melts are extracted they are assumed to advect upward and immediately underplate the crust at the CMTZ. Only the thermal effect of the underplating is taken into account: the sensible and latent heat of the melts is removed from the source regions and used to increase the temperature between $z = 41$ km and $z = 52$ km, that is, distributed within the markers inside the grid element that encloses the CMTZ.

Crustal melts are only extracted if the amount of partial melt exceeds the removal threshold. The used value of 8% for crustal melts represents a liquid percolation threshold (Vigneresse et al., 1996) at which point melt

pockets become connected. Once this threshold is exceeded, all melts are removed. No threshold is imposed for mantle melts; the low viscosity of mantle melts and the high strain rates caused by the sublithospheric small-scale convection (SSC) are assumed to effectively extract mantle melts by stress-driven melt segregation (Kohlstedt & Holtzman, 2009). See section 4 about the effect of these thresholds for the model behavior.

2.3. Model Setup

Figure 1 shows the model setup. An upper mantle model domain with aspect ratio 4 (2,640 × 660 km) is created, in which a thickened crust (45 km) and a total (chemical) lithosphere thickness of 90 km represent the structure of the lithosphere after collision and subsequent rethinning of the lithosphere. The temperature is 0 °C at the surface and fixed at 1690 °C (potential temperature 1360 °C) at the bottom, with zero heat flow at the lateral boundaries. The bottom boundary condition temperature is chosen so that the potential temperature of the convecting mantle is at a realistic level (1330 ± 10 °C). Internal radiogenic heating is constant throughout the model domain and is increased by a factor of 3 compared to real mantle values (cf. Kaislaniemi & van Hunen, 2014). This is done to replace bottom heating by a similar amount of internal heating. This replacement therefore maintains a similar thermal evolution, while suppressing the generation of plume-like upwellings that would be caused by mainly bottom-heated models and that would increase the complexity of the models and, in some cases, would help destabilize the lithospheric mantle. It is likely that the high-viscosity lower mantle helps anchor plumes in one place (Lowman & Gable, 2008). Our models are restricted to the upper mantle only, and thus, other measures are needed to suppress the appearance of plumes. We limit the applicability of our models to environments where plume interaction with the orogenic lithosphere is likely to have been absent. All boundaries have a free-slip velocity boundary condition. The initial density structure (Figure 1) takes into account the upper and lower crust and the lithospheric mantle with a small inherent compositional, depleted-related buoyancy compared to the sublithospheric mantle.

All models are started from an initial premelt model where the thermal lithosphere thickness has reached a statistical steady state, so that the 1250 °C isotherm has located at z =90 km for about 40 Myr. These initial models are run using the model setup from Figure 1 and parameters from the reference model (*M000*, Table 2), with all melting disabled. Once the steady state is reached, melt calculations and parameters according to Table 2 are switched on. In the results shown, this moment has a model time of 0 Myr and is common for all the models.

The water content of the subcontinental lithospheric mantle in postcollisional areas is not well constrained, but several lines of evidence suggest that it is enriched is volatile elements, and especially water. Such enrichment is clearly inherited from the subduction system that preceded collision (e.g., Prelević et al., 2013). A nominally anhydrous mantle contains up to 200-ppm H_2O (Hirschmann, 2006), and in several places xenoliths show widespread and heterogeneous evidence of metasomatism inherited from subduction. The metasomatic character of the mantle is demonstrated by the presence of phlogopite and/or amphibole in mantle xenoliths present in high-K postcollisional mantle melts (e.g., in Tibet; ; Liu et al., 2011) or in recent volcanic centers sampling postorogenic mantle (e.g., in the Massif-Central; ; Lenoir et al., 2000). Although heterogeneously distributed, hydrous phases can amount to as much as 5 wt %, thus making up to 2,000 ppm of H_2O in a phlogopite-bearing mantle. Our models use a value of 400 ppm of H_2O for the mantle, a value above the nominally anhydrous mantle, representing a reasonable estimate of a metasomatic mantle (containing ∼ 2wt% of amphibole or ∼ 1wt% of phlogopite). This hydrous mantle represents conditions in a postcollisional setting where previous subduction has been hydrating the overlying lithospheric mantle and leads to relatively strong localized intermittent and temporary thinning of the lithosphere is, in itself, not enough to destabilize the whole lithospheric mantle (i.e., the average thickness of the thermal lithosphere is constant and reached in the initial premelt model calculations).

For the initial crustal rock composition, we use a global estimate from Rudnick and Fountain (1995) for a general average lower crust composition of platform and shield areas (SiO_2: 52.4; MgO: 7.1; CaO: 9.5; Al_2O_3: 16.5; Na_2O: 2.7; K_2O: 0.6; FeO_T: 8.2; TiO_2: 0.8 wt %) with a water content of 1.5 wt %.

To test the effects of partial lower crust and mantle melting to the lithosphere stability, we have run the models with varying controlling parameters (Table 2).

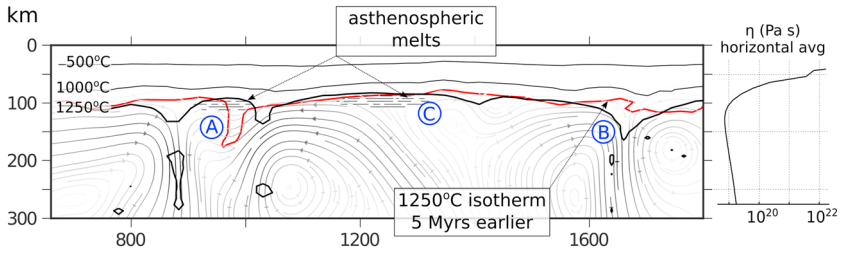

Figure 2. A view on the sublithospheric small-scale convection in early stages of model calculation. Black solid lines are the lithosphere isotherms, black-to-gray lines with arrows describe the velocity field (darker color means higher velocities; maximum velocity is 25mm/year), and the red solid line is the previous location of the 1250 °C isotherm, 5 Myr earlier. High water content, compared to dry mantle, lowers viscosity, enhances convection, and causes the size of the convection cells to decrease to about 100–300 km in diameter. This enhanced convection heats the lithosphere more effectively from below and erodes the bottom of the lithosphere, causing some locations (e.g., A) to have locally decreasing lithosphere thickness, but other locations to increase in lithosphere thickness (e.g., B). The locations of thickened and thinned lithosphere vary in time, so that small-scale convection alone does not lead to removal of the whole lithospheric mantle but instead a thinned (heated) lithosphere is rethickened (cooled) later, and the average lithosphere thickness reaches a steady state value (approximately 100 km in the models here). Some asthenospheric melts may appear temporarily in places where lithosphere is thinned (crosses near A and C; cf. Kaislaniemi et al., 2014). Horizontal average of the effective viscosity is shown on the right.

3. Results

A complex interplay between melt weakening, depletion stiffening, and chemical depletion can be observed in the models (Figure 2). The model setup in the initial premelt model leads to a (statistical) steady state where the lithosphere thickness is locally and temporally thinned and then thickened again. The locations of these thinned and thickened regions vary through time. This is caused by the sublithospheric SSC that is enhanced by the elevated water concentrations in the mantle.

After this initial *premelt* model, the behavior of the models depends on the used parameters (Table 2). In reference model *M000*, melt amounts are calculated but do not affect the flow (Figures 3a–3d): melt does not weaken the material and is not extracted. This model continues to produce SSC, and the average lithosphere thickness does not change. Partial melting takes place in the lowermost crust, with increased degree above locally thinned lithosphere. At the same time, some asthenospheric melts are produced by decompression melting below the thinned locations. As the melts are not removed, they will solidify once the SSC pattern changes and lowers the geotherm again.

In models where melt weakening is enabled (*M1xx*), partial crustal and asthenospheric melting leads to a decrease in the viscosity. This weakening produces a positive feedback (Figures 3e–3h) where melt weakening sustains further thinning of the lithosphere—leading to complete removal of the lithospheric mantle—and thus also higher total amounts of both crustal and mantle melts as compared to model *M000*. Such complete removal of the lithospheric mantle takes place as *dripping* of the lithosphere into the asthenosphere and is more akin to (fast) convective thinning, or foundering as drips, than to delamination as one coherent layer (Bird, 1979).

The removal of the lithospheric mantle in model *M100* (Figures 3e–3h) takes approximately 20 Myr, changing from almost intact mantle lithosphere at about 50-Myr model time to completely absent mantle lithosphere, spanning 200 km horizontally, at 70 Myr. The timing and location of this event is, to some extent, random: it is triggered by the SSC, which itself is chaotic in a sense that the convection cells that locally thicken and thin the lithosphere move horizontally in a random pattern. Whenever the lithosphere happens to be thinned strongly enough for long enough time to raise the geotherm at lower crustal levels, the complete, *catastrophic*, foundering of mantle lithosphere can start. Despite the randomness caused by SSC, the overall convective thinning of the lithosphere has a systematic control on timing and location of the full mantle lithosphere removal: once the global lithosphere thickness has decreased to level that small local perturbations start to affect crustal temperatures, complete foundering has a chance to start.

3.1. Mantle Input

When underplating of mantle melts at CMTZ is enabled in the models (*M110*, Figure 4), this is found to initially increase the crustal melting rate, but to decrease the total amount of crustal melting. This is caused by changes

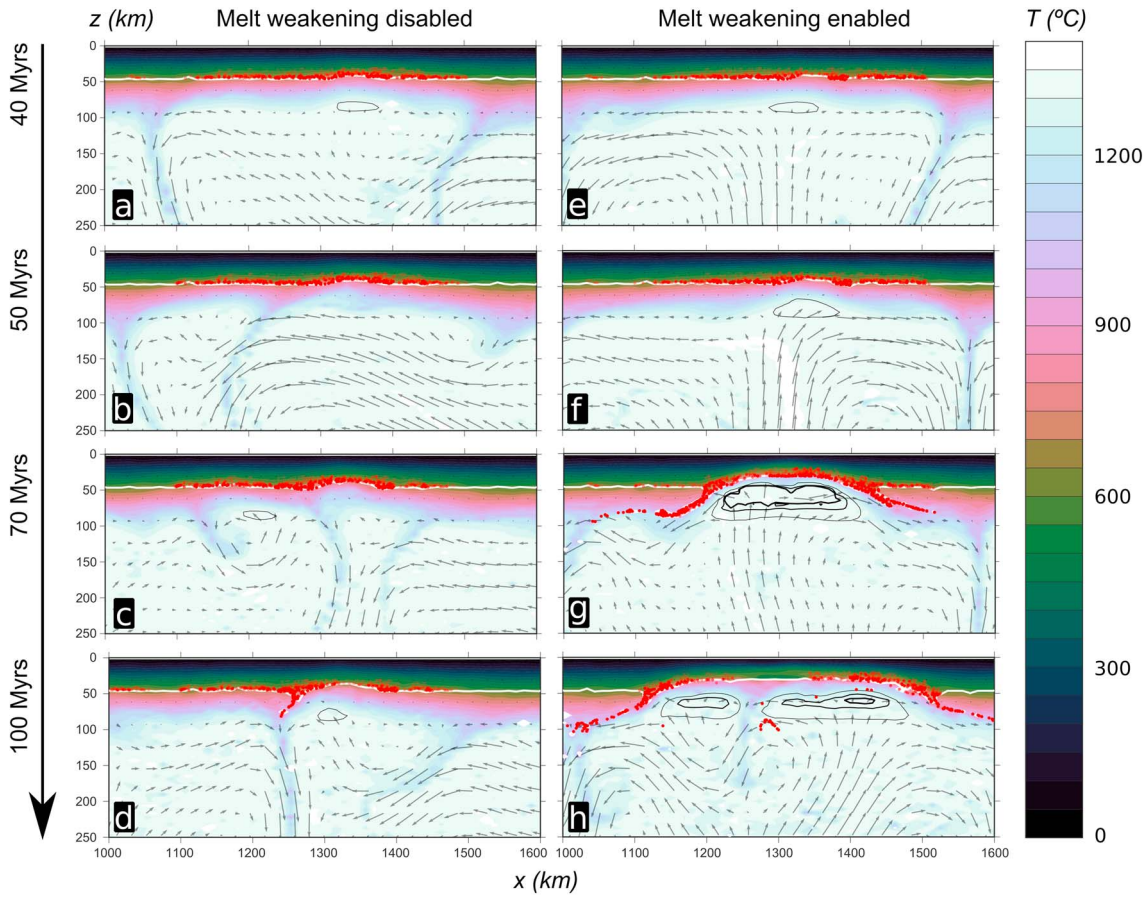

Figure 3. Comparison of models with melt weakening effects disabled (a–d, model M000) and enabled (e–h, model *M100*). Background colors describe the temperature field. Red dots indicate markers of crustal lithology with more than zero partial melt. Melt weakening (e–h) leads to positive feedback and enhanced lithospheric thinning (f) and eventually to complete removal of the lithospheric mantle (g, h). White contour shows the crust-mantle transition zone, the lithological boundary between crust and mantle. Black contours show degree of mantle melting (1%, 3%, and 5%). Velocity arrows scale with the axes (km/Myr).

in the melt source regions: Once the mantle melts are extracted and advected to the CMTZ, the residue left in the mantle is low in water content, since most of the water was partitioned in the melt. This melt-depleted mantle has a higher viscosity than the fertile mantle. At the same time, the weakening of the residue caused by the presence of melts disappears (as the melts are drained away). Removing water from the mantle rock also makes it more refractory and production of further mantle melts is hindered. Additionally, the depleted peridotite is less dense than fertile peridotite. All these effects accumulate to cause the mantle source region for the underplating melts to become a layer of high-viscosity, buoyant and refractory material. This stops the thinning of the lithosphere and *shields* the crust and remaining lithospheric mantle from the hot convecting mantle below. The foundering ends and the lithosphere starts to cool and thicken again, so that the layer of depleted mantle material becomes part of the stable lithosphere.

If there is no underplating of the mantle melts at the CMTZ but melts are left in their place within the mantle (*M100*), the viscosity remains low because of the melt weakening effect of the melts. Initial amounts of crustal melting are not increased by the advection of heat from the melts. However, the foundering is driven further by the presence of the low-viscosity mantle melts and will spread horizontally to span more than 400 km. Additionally, the lithosphere regains its thickness very slowly, extending the time the lower crust is exposed to the hot convecting mantle. This leads to prolonged times of crustal melting. Extraction of the crustal melts (in *M111*) has a similar negative feedback effect on any further crustal melting, because melt removal leaves a residue that is more refractory in composition (Figures 5d and 5e).

3.2. Melt Production

The models where melt weakening is enabled, and most of the mantle lithosphere is removed, show a characteristic pattern of melt production. In model *M111*, where both crustal and mantle melts are extracted, minor

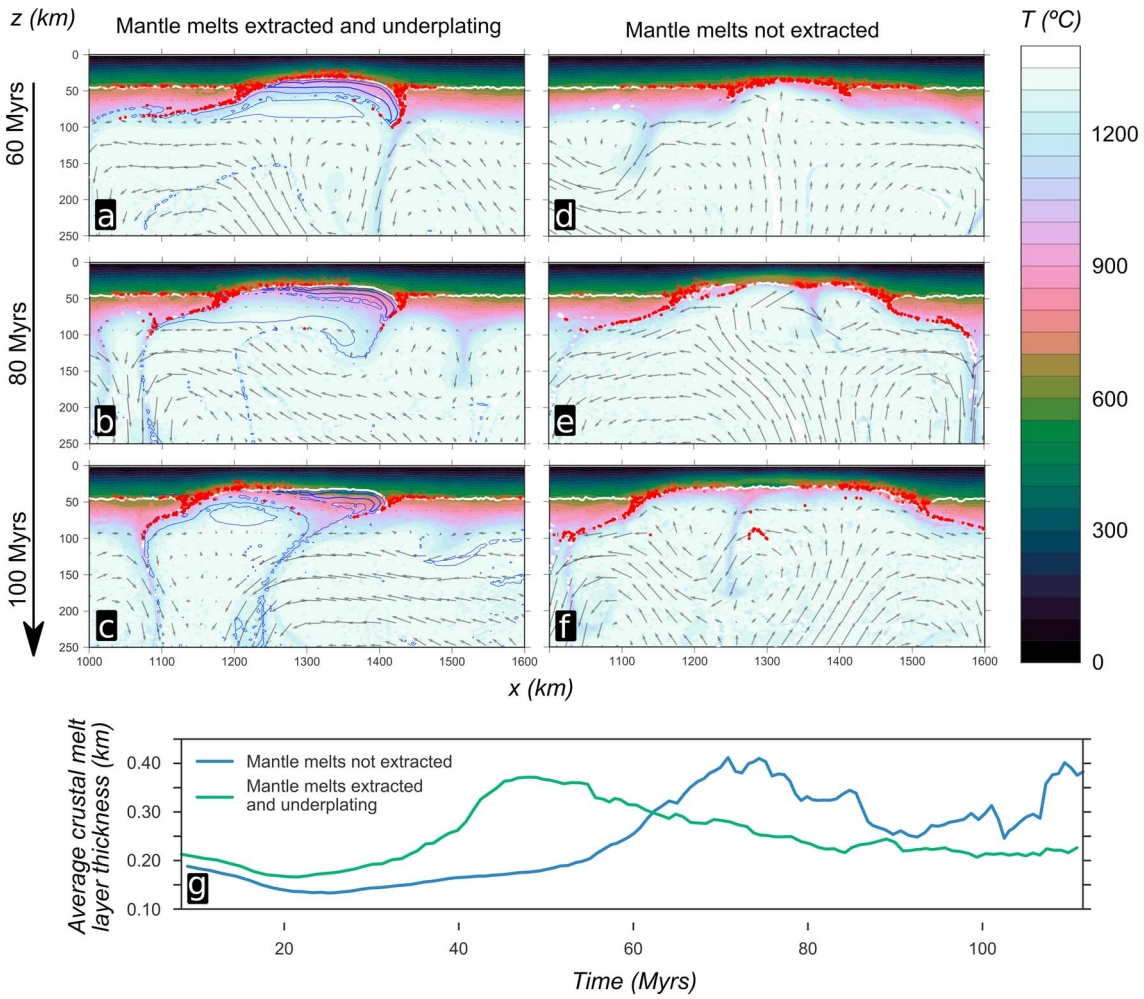

Figure 4. In models where mantle melts are extracted and underplate the crust at crust-mantle transition zone (model M110, a–c) a high-viscosity buoyant residue layer is formed underneath the crust (blue contours, 1%, 3%, and 5% melt depletion). This protects the lithosphere from further thinning and allows it to cool back to its original thickness (c). If mantle melts are not extracted (model M100, d–f) foundering of the lithospheric mantle continues longer and extends over broader region. Plot of horizontally averaged crustal melt amount across section x = 1,000–1,600 km (g) shows that underplating initially promotes crustal melting (green line) but eventually slows down as compared to without underplating (blue line). Note that the decrease in the melt amount is possible since the crustal melts are not extracted and may thus recrystallize. Velocity arrows scale with the axes (km/Myr).

amounts of partial melts, that is, summed layer thickness up to maximum of 500 m, exist in the lowermost crust before the lithospheric mantle is foundered into the asthenosphere (Figures 5a and 5d). The degree of melting is initially not large enough to extract any melt (Figure 5b, before 25 Myr). As the SSC produces a locally thinned region of lithosphere, the hot convecting mantle moves closer to the lowermost crust, producing more crustal melts. This initiates the discussed positive feedback mechanism, as seen in model *M100*, leading to further thinning and melting. The degree of crustal melts exceeds the liquid percolation threshold and the crustal melts can be extracted (Figure 5b, after 25 Myr). Once the crustal melts are extracted, the refractory residue does not melt further, and the production of crustal melts slowly disappears. The convecting mantle, however, still drags pieces of crust horizontally and then down deeper into the mantle, forming *tracks* of crustal melting taking place at the boundaries of the extremely thin mantle lithosphere, spreading horizontally as the region of foundering lithosphere expands.

At the culmination of the mantle lithosphere removal, when the hot convecting mantle comes in direct contact with the crust, there is a single pulse of crustal melting and melt extraction (Figure 5b, at 50 Myr, x = 1,350 km), lasting 5 to 10 Myr. Shortly prior to this, at ~ 43 Myr, a strong pulse of mantle melting commences. This pulse of mantle melts, although fading, continues for up to 30 Myr, since the convection can replace some of the depleted mantle with fertile material from below.

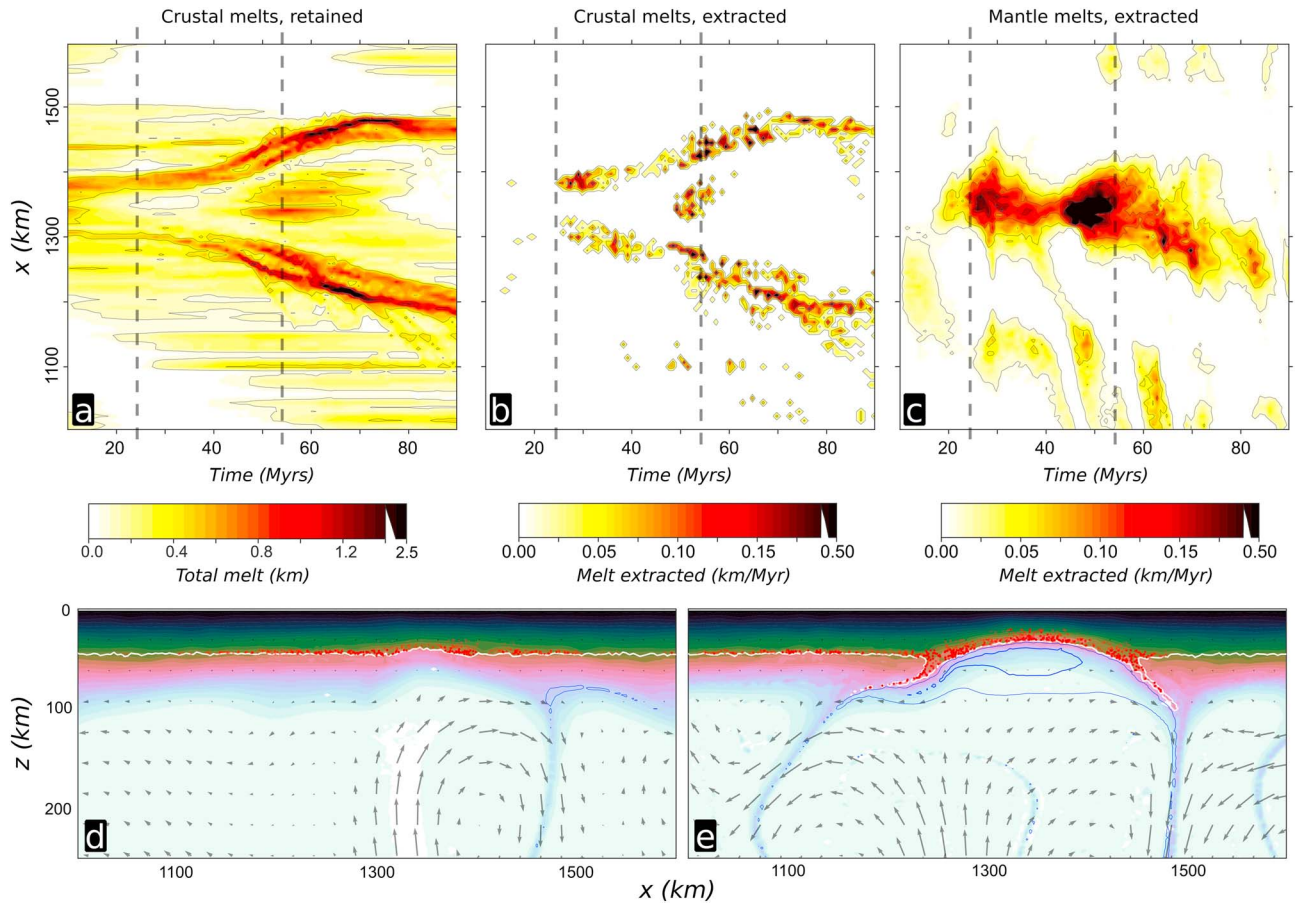

Figure 5. Spatiotemporal evolution of crustal and mantle melting in model M111. Melt amount is measured as an imaginary layer thickness the melts would form if gathered into one layer (i.e., vertically integrated melt volume divided by surface area). Melt extraction rates are measured as a change over time in this layer thickness. (a) Total amount of unextracted crustal melts, not exceeding the extraction threshold, that is, present within the crust. (b) Flux of crustal melts exceeding the extraction threshold and extracted. (c) Flux of mantle melts formed and extracted (extraction threshold is zero for mantle melts). Note the different scale between (a) and (b) and (c). (d, e) Model snapshots at times marked with dashed lines in (a)–(c) (25 and 55 Myr). Red dots show presence of crustal melts; blue contours show degree of melt depletion in the mantle (1%, 3%). Temperature color and velocity scale as in Figure 3.

4. Discussion

Our results indicate significant interactions between mantle and crustal processes as the destabilization of the orogenic lithosphere proceeds. We show how sublithospheric SSC increases mantle heat flow into the lower crust enough to trigger minor crustal anatexis which may, via positive feedback effects, result in catastrophic foundering of the whole mantle lithosphere into the asthenosphere. A prerequisite for this to happen is a lithosphere that has reached close its original thickness after collision, and a moderately elevated water contents in the upper mantle.

From these results, we can better understand the formation of granite-migmatite belts in the frame of post-collisional settings and propose a model that characterizes the roles of the mantle and the crust: Convective thinning of the orogenic thickened lithosphere brings the lithosphere closer to its original thickness. Thermal relaxation and subsequent increased basalt heat flow by the sublithospheric SSC leads to higher temperatures in the crust and uppermost lithospheric mantle, as well, and increases temperatures above the solidus at the lower level of the thickened crust, starting the formation of migmatites. These partial melts in the lower crust may exist for prolonged times. The nature of the SSC causes variation in the degree of melting, and the rheological weakening by the partial melts can trigger foundering of the whole lithospheric mantle in places where amount of partial melts is high enough. The water initially introduced by subduction into the overriding plate through metasomatism allows the initiation of SSC, and (conceptually) also added to the convective thinning prior to its initiation.

Removal of the mantle lithosphere leads to strong asthenospheric upwelling and extensive melting by decompression where the lithosphere is thinnest. Within about 20–30 Myr the lower crust is exposed to the asthenosphere over a distance of a few hundred kilometers. There is a significant increase in the lower crustal melting. This pulse of crustal melt formation continues for about 5–10 Myr. The degree of melting in the crust rises above the critical threshold of melt extraction, which would ultimately trigger the formation of granitic plutons in higher crustal levels. This process can explain the generation of postcollisional granite-migmatite zones showing long-lived anatectic crust followed by extensive melt extraction and emplacement associated with mantle-derived magmatism. The crustal melting stops rather abruptly, and the mantle-derived magmatism slowly wanes as the lithosphere grows back to its steady state thickness. As a result of this whole process, mantle melts are temporally related to crustal melting but have different spatial distribution (cf. Figures 5b and 5c).

4.1. Relation to Observed Late-Orogenic Magmatism

This scenario fits the temporal and petrogenetic relations between the migmatites, granitic plutons, and mafic bodies produced at late stages of many orogenic collisions. The granitic suites (Bonin, 2004) of crustal origin are typically associated with postcollisional mafic magmas that are rich in both compatible (Mg, Fe, Ni, and Cr) and incompatible elements (K_2O, high-field-strength elements, and light rare-earth elements; e.g., Castro et al., 2003; Fowler, 1988; Fowler & Rollinson, 2012; Graessner et al., 2000; Kotkova et al., 2010; Molina et al., 2012; Murphy, 2013). They are most often deduced to have their sources in the lithospheric mantle that has been enriched by incompatible crustal components during the subduction. These postcollisional mafic magmas are coeval or slightly predate the granitic plutonism, both of which, in turn, postdate crustal anatexis of variable durations (in some cases with considerable overlap). This is the case, for example, in the Canadian Cordillera (Gordon et al., 2008) with 20 Myr of progressive gneiss-migmatite formation ending in a short pulse of leucogranite plutonism; in the Proterozoic Svecofennian orogeny (Väisänen et al., 2000) where shoshonitic mantle melts intervene the granite-migmatite belt formation over 20 Myrs; in the Variscan orogeny in central Spain (Montero et al., 2004) and in Calabria (Graessner et al., 2000); and, as a well studied example, the Velay dome region of the eastern French Massif Central (Couzinié et al., 2014; Laurent et al., 2017).

The Velay dome granite-migmatite complex is one of the best studied examples of a large-scale anatectic system that developed in a late orogenic stage. It hosts abundant and diverse granitoid rocks that have been emplaced at the end of the collision and throughout the late-orogenic collapse. These granitoids are formed in two stages (Laurent et al., 2017): (1) metamorphism and limited, water-present partial melting during 340–314 Ma, and (2) high-temperature, extensive biotite breakdown melting at 310–300 Ma, finally leading to the collapse and formation of the Velay dome itself at 305–300 Ma. These granitoids are sourced from the orthogneisses and paragneisses of the local orogenic crust and have been measured with *P-T* conditions of 5–6 kbar, 720–750 °C, and 4–5 kbar, 750–850 °C, for the two stages, respectively (Barbey et al., 1999; Bouilhol et al., 2006; Couzinié et al., 2014; Montel et al., 1992; Mougeot et al., 1996). Volumetrically minor enclaves of gabbroic to dioritic rocks, vaugnerites, are ubiquitously hosted within the granitoids. The vaugnerites have high-K to shoshonitic affinities and are rich in incompatible trace elements, taken as evidence for having their source in the metasomatized lithospheric mantle (Couzinié et al., 2016). The vaugnerites are generated throughout the 340–300 Ma period but seem to have a peak in their generation rate at circa 315–305 Ma (Couzinié et al., 2014; Laurent et al., 2017), slightly before the collapse and formation of the Velay dome. The 40 Myr period of sustained high heat flux and crustal anatexis requires a long-lived thermal anomaly, and, also, a mechanism to explain the incubation period of 340–310 Ma before the more extensive melt production commences. The apparent lack of orogenic root underneath the eastern French Massif Central (Averbuch & Piromallo, 2012) suggests that removal of the lithospheric mantle after the collision could have contributed this extra heating. We suggest that our model presented above provides the mechanism for this mantle lithosphere removal and explains the spatiotemporal relations of the mantle and crustal melts in the Velay dome granite-migmatite complex. The mantle melts of our models represent the vaugnerite magmatism, and the lower crustal melts directly and indirectly, via advective heating, contribute to the granitic magmatism and increased geotherm at the upper crustal levels.

Our model agrees well with the above-mentioned observations from the Velay dome region of the Variscan orogeny but could be more generally applied to other orogenies that show marks of orogenic collapse, as well. The new model for the formation of orogenic granite-migmatite belts presented here shows the importance of the interaction between mantle and crustal processes and suggests less straightforward cause-and-effect relationships than existing conceptual models: the asthenospheric upwelling associated with the orogenic

collapse is not a passive upwelling caused by the lithospheric extension, nor does it need to be the primary initiator of the high-temperature metamorphism of the lower crust, as commonly suggested (e.g., Liu & Shen, 1998; Sonder & Jones, 1999). Instead, in our models, such upwelling postdates the beginning of the crustal anatexis that is initiated by convective downwellings that thin the lithosphere by SSC and plays an important role only once the lower crust is sufficiently weakened by the partial melts. Though dating of these prograde metamorphic events from the geological record might prove difficult for geochronology, we note that the mantle-derived magmatism intervening crustal plutonism requires some concurrency of mantle and crustal melt extraction. This requirement is fulfilled in the described model. Dome-like structures at the bottom of the crust can be formed after the foundering of the lithospheric mantle (cf. Figure 5e) causing lateral variation in the degree of partial melting within the crust.

4.2. Feedback Mechanisms

The extraction rates of mantle and crustal melts are critical for the positive feedback effect between melt weakening and lithosphere removal to work. If all crustal melts are extracted at the same rate as they form, there will be no melt present in the lower crust to cause the rheological weakening, and thus, the positive feedback effect is disabled. Immediate extraction of mantle melts does not have an equally dramatic effect, although retention of mantle melts does favor stronger thinning of the lithosphere and more extensive lower crust melting. Consequently, the process of granite-migmatite belt formation, mantle lithosphere detachment, and orogenic collapse can be brought to a halt by early melt extraction. Variations in melting history (fast/slow production of melts) and/or in melt extraction threshold values (lithology, deformation-enhanced extraction) could perhaps explain why some orogenies (e.g., Uralides and Trans-Hudson orogeny) have not experienced orogenic collapse but instead have a structure of an arrested orogeny with relatively thick crust underlain by mechanically intact lithosphere (Artemieva & Mooney, 2001; Leech, 2001). Strength increase due to early melt extraction might provide a mechanism for stopping a self-sustaining delamination process also in other settings. Further studies are needed to resolve how sensitive the initiation and halting of full mantle lithosphere removal is to melt extraction rates. Our models used melt percolation thresholds of 8% (for crustal rocks) and 0/∞% (for mantle rocks). These values directly affect the melt extraction rates, and variation in these values is likely to affect the behavior of the models: Higher percolation thresholds will allow the mantle lithosphere removal to progress further before melt removal slows down the process (cf. models M100 and M110).

Underplating of mafic magmas from the mantle at the CMTZ has been suggested to promote crustal melting (Annen & Sparks, 2002; Laube & Springer, 1998; Petford & Gallagher, 2001). However, in order to produce observed melt volumes within the crust, enough heat must be transferred from the mantle. This requires semi-continuous or periodic underplating of mantle melts. Our results indicate that this supply is dependent on the processes that take place at the lithosphere-asthenosphere boundary. Advection of underplating magmas leaves behind a residue that diminishes further supply of melts. This process is sensitive to the amount of water in the mantle: high water content causes more extensive mantle melting, and thus higher amounts of underplating and crustal melting, and also stronger contrasts in viscosity and buoyancy between the fertile mantle and the depleted mantle. The *shielding* layer of this depleted mantle will be more effective in this case and will prevent further mantle melting and underplating efficiently. Our parameterization of density decrease as a function of melt depletion follows Schutt and Lesher (2006) who considered dry phases. If removal of light hydrous phases (mica and amphibole) from the residue would lead to its density increase instead, this would lead to less buoyant layer of depleted *shield*, and possible faster or more extensive removal of the lithospheric mantle. The depleted shielding layer is likely to form, anyway, at some later point, after the consumption of hydrous phases from the source.

Our models show that purely mantle-dominated processes can cause crustal anatexis assuming postcollisional SSC at the asthenosphere-lithosphere boundary and the positive feedback between mantle/crustal melting and further lithosphere thinning by melt weakening. Other processes suggested to be the heat source for granite-migmatite belt formation, such as increased radiogenic heating in the thickened crust, are not necessary. Should they take place, however, their effect would promote the crustal melting but would not remove the positive feedback effect between melting and lithosphere thinning observed in our models. For example, Maierová et al. (2016) used crustal scale numerical models to study the gravitational overturn of the thickened orogenic crust in hot, large orogens, such as the European Variscides, with a relaminated felsic lower crust. They showed that the gravity overturn happens even with minor gravity inversion in the crust and that the consequent exhumation of the lower crust is enhanced by rheological weakening due to partial melting. Our models have significantly less detailed description of the crust, but these results can be seen as

complementary to each other: The mantle processes described here provide additional heat for the melting of the (lower) crust, and buoyancy-driven exchanges within the crust described by Maierová et al. (2016) form the final crustal structure of the orogen with the heterogeneous, partially molten, middle crust and its polyphase tectonic history. Similarly, even though a postcollisional slab break-off at shallow level could be a potential cause for increased basal heating of the crust, our results show that it is not necessary to explain the crustal anatexis and mafic magmatism.

5. Conclusions

We have investigated numerically the sensitivity of lithosphere stability to melt-induced weakening in a postcollisional lithosphere. Our models show that partial melting of the lowermost crust—caused by the increased geotherm by convective thinning of the lithosphere and sublithospheric SSC underneath it—can lead to positive feedback by melt weakening and to the foundering of the whole lithospheric mantle in to the asthenosphere, leading to mantle- and crust-derived late-orogenic magmatic activity.

This process explains the generation of those granite-migmatite zones that show long-lived partial melting of the crust followed by extensive plutonism and intervening mantle-derived magmatism. Furthermore, it provides an explanation for the observed relationships between asthenospheric upwelling, extension, and orogenic collapse following crustal anatexis: the orogenic collapse need not to be driven by the asthenospheric upwelling or the partial melts in the crust formed during the collision. Instead, thinning of the thickened orogenic lithosphere is enhanced by fluids in the asthenosphere, subducted during and before the collision, leading to increased geotherm and partial melting of the lower crust. Partial melts weaken the lithosphere and drive further thinning, and thus further melting. This positive feedback causes loss of lithospheric mantle and extensive crustal melting, both of which drive orogenic collapse. Progressive removal of the lithospheric mantle provides a heat source for the crustal anatexis, and simultaneously explains the generation of late-orogenic mantle-derived magmas.

Underplating of mantle-derived melts below the crust is found to increase initial crustal melting rates, but to have a close-to-neutral effect in overall crustal melting on timescales of the whole collision and postcollisional relaxation. The source regions of these underplating melts become refractory and form a high-viscosity layer that inhibits further mantle melting and brings lithosphere foundering to a halt.

Acknowledgments
L. K. acknowledges funding from European Union Marie Curie Initial Training Network "Topomod" (project 264517). J. vH. and P. B. acknowledge funding from the European Research Council (ERC StG 279828). We would like to thank Kosuke Ueda, Claire Currie, and Tanya Furman for their thorough and beneficial reviews. Detailed method description and derivation of the viscosity parameterization prior to melt weakening extension can be found in Kaislaniemi et al. (2014) and its appendix, GSA Data Repository 2014110, (DOI:10.1130/G35193.1).

References

Annen, C., & Sparks, R. S. J. (2002). Effects of repetitive emplacement of basaltic intrusions on thermal evolution and melt generation in the crust. *Earth and Planetary Science Letters*, *203*(3-4), 937–955. https://doi.org/10.1016/s0012-821x(02)00929-9

Artemieva, I. M., & Mooney, W. D. (2001). Thermal thickness and evolution of precambrian lithosphere: A global study. *Journal of Geophysical Research*, *106*(B8), 16,387–16,414. https://doi.org/10.1029/2000jb900439

Averbuch, O., & Piromallo, C. (2012). Is there a remnant variscan subducted slab in the mantle beneath the paris basin? Implications for the late Variscan lithospheric delamination process and the Paris basin formation. *Tectonophysics*, *558-559*, 70–83. https://doi.org/10.1016/j.tecto.2012.06.032

Barbey, P., Marignac, C., Montel, J. M., Macaudière, J., Gasquet, D., & Jabbori, J. (1999). Cordierite growth textures and the conditions of genesis and emplacement of crustal granitic magmas: The Velay granite complex (massif central, France). *Journal of Petrology*, *40*(9), 1425–1441. https://doi.org/10.1093/petroj/40.9.1425

Bea, F. (2012). The sources of energy for crustal melting and the geochemistry of heat-producing elements. *Lithos*, *153*, 278–291. https://doi.org/10.1016/j.lithos.2012.01.017

Bird, P. (1979). Continental delamination and the Colorado plateau. *Journal of Geophysical Research*, *84*(B13), 7561–7571. https://doi.org/10.1029/jb084ib13p07561

Bonin, B. (2004). Do coeval mafic and felsic magmas in post-collisional to within-plate regimes necessarily imply two contrasting, mantle and crustal, sources? A review. *Lithos*, *78*(1-2), 1–24. https://doi.org/10.1016/j.lithos.2004.04.042

Bouilhol, P., Leyreloup, A. F., Delor, C., Vauchez, A., & Monié, P. (2006). Relationships between lower and upper crust tectonic during doming: The mylonitic southern edge of the Velay metamorphic core complex (cévennes-French massif central). *Geodinamica Acta*, *19*(3-4), 137–153. https://doi.org/10.3166/ga.19.137-153

Bouilhol, P., Magni, V., van Hunen, J., & Kaislaniemi, L. (2015). A numerical approach to melting in warm subduction zones. *Earth and Planetary Science Letters*, *411*, 37–44. https://doi.org/10.1016/j.epsl.2014.11.043

Brown, M. (2001). Orogeny, migmatites and leucogranites: A review. *Journal of Earth System Science*, *110*(4), 313–336. https://doi.org/10.1007/bf02702898

Burov, E. B., & Watts, A. B. (2006). The long-term strength of continental lithosphere: "Jelly sandwich" or "crème brûlée"? *GSA Today*, *16*(1), 4. https://doi.org/10.1130/1052-5173(2006)016<4:tltsoc>2.0.co;2

Castro, A., Corretgé, L. G., Rosa, J. D. d. l., Fernandéz, C., López, S., & Garciá-Moreno, C. H. (2003). The appinite-migmatite complex of Sanabria, NW Iberian massif, Spain. *Journal of Petrology*, *44*(7), 1309–1344. https://doi.org/10.1093/petrology/44.7.1309

Christensen, U. R., & Yuen, D. A. (1985). Layered convection induced by phase transitions. *Journal of Geophysical Research*, *90*(B12), 10,291–10,300. https://doi.org/10.1029/jb090ib12p10291

Chung, S.-L., Liu, D., Ji, J., Chu, M.-F., Lee, H.-Y., Wen, D.-J., et al. (2003). Adakites from continental collision zones: Melting of thickened lower crust beneath southern tibet. *Geology*, *31*(11), 1021–1024. https://doi.org/10.1130/g19796.1

Connolly, J. A. D. (2005). Computation of phase equilibria by linear programming: A tool for geodynamic modeling and its application to subduction zone decarbonation. *Earth and Planetary Science Letters*, *236*(1-2), 524–541. https://doi.org/10.1016/j.epsl.2005.04.033
Connolly, J. A. D. (2009). The geodynamic equation of state: What and how. *Geochemistry, Geophysics, Geosystems*, *10*, Q10014. https://doi.org/10.1029/2009gc002540
Couzinié, S., Laurent, O., Moyen, J.-F., Zeh, A., Bouilhol, P., & Villaros, A. (2016). Post-collisional magmatism: Crustal growth not identified by zircon Hf isotopes. *Earth and Planetary Science Letters*, *456*, 182–195. https://doi.org/10.1016/j.epsl.2016.09.033
Couzinié, S., Moyen, J.-F., Villaros, A., Paquette, J.-L., Scarrow, J. H., & Marignac, C. (2014). Temporal relationships between Mg-K mafic magmatism and catastrophic melting of the Variscan crust in the southern part of Velay complex (massif central, France). *Journal of GEOsciences*, *59*(1), 69–86. https://doi.org/10.3190/jgeosci.155
Davies, J. H., & von Blanckenburg, F. (1995). Slab breakoff: A model of lithosphere detachment and its test in the magmatism and deformation of collisional orogens. *Earth and Planetary Science Letters*, *129*(1-4), 85–102. https://doi.org/10.1016/0012-821x(94)00237-s
Dewey, J. F. (1988). Extensional collapse of orogens. *Tectonics*, *7*(6), 1123–1139. https://doi.org/10.1029/tc007i006p01123
Finger, F., Gerdes, A., Renó, M., & Riegler, G. (2009). The saxo-danubian granite belt: Magmatic response to post-collisional delamination of mantle lithosphere below the southwestern sector of the bohemian massif (Variscan orogen). *Geologica Carpathica*, *60*(3). https://doi.org/10.2478/v10096-009-0014-3
Fowler, M. B. (1988). Ach'uaine hybrid appinite pipes: Evidence for mantle-derived shoshonitic parent magmas in caledonian granite genesis. *Geology*, *16*(11), 1026–1030. https://doi.org/10.1130/0091-7613(1988)016<1026:AUHAPE>2.3.CO;2
Fowler, M., & Rollinson, H. (2012). Phanerozoic sanukitoids from caledonian scotland: Implications for archean subduction. *Geology*, *40*(12), 1079–1082. https://doi.org/10.1130/G33371.1
Franke, W. (2000). The mid-European segment of the variscides: Tectonostratigraphic units, terrane boundaries and plate tectonic evolution. *Geological Society, London, Special Publications*, *179*(1), 35–61. https://doi.org/10.1144/gsl.sp.2000.179.01.05
Fuhrman, M. L., & Lindsley, D. H. (1988). Feldspar minerals. *Amer Miner*, *73*, 201–215.
Gerya, T. V., & Meilick, I. (2011). Geodynamic regimes of subduction under an active margin: Effects of rheological weakening by fluids and melts. *Journal of Metamorphic Petrology*, *29*, 7–31. https://doi.org/10.1111/j.1525-1314.2010.00904.x
Gerya, T. V., & Yuen, D. A. (2003). Characteristics-based marker-in-cell method with conservative finite-differences schemes for modeling geological flows with strongly variable transport properties. *Physics of the Earth and Planetary Interiors*, *140*(4), 293–318. https://doi.org/10.1016/j.pepi.2003.09.006
Göğüş, O. H., & Pysklywec, R. N. (2008). Mantle lithosphere delamination driving plateau uplift and synconvergent extension in eastern Anatolia. *Geology*, *36*(9), 723–726. https://doi.org/10.1130/g24982a.1
Göğüş, O. H., Pysklywec, R. N., Şengör, A. M. C., & Gün, E. (2017). Drip tectonics and the enigmatic uplift of the Central Anatolian Plateau. *Nature Communications*, *8*, 1538. https://doi.org/10.1038/s41467-017-01611-3
Gordon, S. M., Whitney, D. L., Teyssier, C., Grove, M., & Dunlap, W. J. (2008). Timescales of migmatization, melt crystallization, and cooling in a cordilleran gneiss dome: Valhalla complex, southeastern British Columbia. *Tectonics*, *27*, TC4010. https://doi.org/10.1029/2007tc002103
Graessner, T., Schenk, V., Bröcker, M., & Mezger, K. (2000). Geochronological constraints on the timing of granitoid magmatism, metamorphism and post-metamorphic cooling in the Hercynian crustal cross-section of Calabria. *Journal of Metamorphic Geology*, *18*, 409–421. https://doi.org/10.1046/j.1525-1314.2000.00267.x
Gray, R., & Pysklywec, R. N. (2012). Geodynamic models of mature continental collision: Evolution of an orogen from lithospheric subduction to continental retreat/delamination. *Journal of Geophysical Research*, *118*, B03408. https://doi.org/10.1029/2011JB008692
Hirschmann, M. M. (2006). Water, melting and the deep earth H_2O cycle. *Annual Review of Earth and Planetary Sciences*, *34*(1), 629–653. https://doi.org/10.1146/annurev.earth.34.031405.125211
Holland, T., & Powell, R. (1991). A compensated-redlich-kwong (CORK) equation for volumes and fugacities of CO_2 and H_2O in the range 1 bar to 50 kbar and 100–1600°C. *Contributions to Mineralogy and Petrology*, *109*(2), 265–273. https://doi.org/10.1007/bf00306484
Holland, T. J. B., & Powell, R. (1998). An internally consistent thermodynamic data set for phases of petrological interest. *Journal of Metamorphic Geology*, *16*(3), 309–343. https://doi.org/10.1111/j.1525-1314.1998.00140.x
Jackson, J. (2002). Strength of the continental lithosphere: Time to abandon the jelly sandwich? *GSA Today*, *12*(9), 4–10. https://doi.org/10.1130/1052-5173(2002)012<0004:sotclt>2.0.co;2
Jamieson, R. A., Beaumont, C., Medvedev, S., & Nguyen, M. H. (2004). Crustal channel flows: 2. Numerical models with implications for metamorphism in the Himalayan-Tibetan orogen. *Journal of Geophysical Research*, *109*, B06407. https://doi.org/10.1029/2003jb002811
Kaislaniemi, L., & van Hunen, J. (2014). Dynamics of lithospheric thinning and mantle melting by edge-driven convection: Application to moroccan atlas mountains. *Geochemistry, Geophysics, Geosystems*, *15*, 3175–3189. https://doi.org/10.1002/2014GC005414
Kaislaniemi, L., van Hunen, J., Allen, M. B., & Neill, I. (2014). Sublithospheric small-scale convection—A mechanism for collision zone magmatism. *Geology*, *42*(4), 291–294. https://doi.org/10.1130/g35193.1
Katz, R. F., Spiegelman, M., & Langmuir, C. H. (2003). A new parameterization of hydrous mantle melting. *Geochemistry, Geophysics, Geosystems*, *4*(9), 1073. https://doi.org/10.1029/2002gc000433
Kohlstedt, D. L., Evans, B., & Mackwell, S. J. (1995). Strength of the lithosphere: Constraints imposed by laboratory experiments. *Journal of Geophysical Research*, *100*(B9), 17,587–17,602. https://doi.org/10.1029/95jb01460
Kohlstedt, D. L., & Holtzman, B. K. (2009). Shearing melt out of the earth: An experimentalist' perspective on the influence of deformation on melt extraction. *Annual Review of Earth and Planetary Sciences*, *37*(1), 561–593. https://doi.org/10.1146/annurev.earth.031208.100104
Kotkova, A., Schaltegger, U., & Lechmann, J. (2010). Two types of ultrapotassic plutonic rocks in the bohemian massif—Coeval intrusions at different crustal levels. *Lithos*, *115*(1-4), 163–176. https://doi.org/10.1016/j.lithos.2009.11.016
Laube, N., & Springer, J. (1998). Crustal melting by ponding of mafic magmas: A numerical model. *Journal of Volcanology and Geothermal Research*, *81*(1-2), 19–35. https://doi.org/10.1016/s0377-0273(97)00072-3
Laurent, O., Couzinié, S., Zeh, A., Vanderhaeghe, O., Moyen, J.-F., Villaros, A., et al. (2017). Protracted, coeval crust and mantle melting during Variscan late-orogenic evolution: U-Pb dating in the eastern French massif central. *International Journal of Earth Sciences*, *106*, 421–451. https://doi.org/10.1007/s00531-016-1434-9
Ledru, P., Courrioux, G., Dallain, C., Lardeaux, J. M., Montel, J. M., Vanderhaeghe, O., & Vitel, G. (2001). The Velay dome (French massif central): Melt generation and granite emplacement during orogenic evolution. *Tectonophysics*, *342*(3-4), 207–237. https://doi.org/10.1016/s0040-1951(01)00165-2
Leech, M. L. (2001). Arrested orogenic development: Eclogitization, delamination, and tectonic collapse. *Earth and Planetary Science Letters*, *185*(1-2), 149–159. https://doi.org/10.1016/s0012-821x(00)00374-5
Lenoir, X., Garrido, C. J., Bodinier, J.-L., & Dautria, J.-M. (2000). Contrasting lithospheric mantle domains beneath the massif central (France) revealed by geochemistry of peridotite xenoliths. *Earth and Planetary Science Letters*, *181*(3), 359–375. https://doi.org/10.1016/S0012-821X(00)00216-8

Liu, M., & Shen, Y. (1998). Crustal collapse, mantle upwelling, and cenozoic extension in the North American Cordillera. *Tectonics*, *17*(2), 311–321. https://doi.org/10.1029/98tc00313
Liu, C.-Z., Wu, F.-Y., Chung, S.-L., & Zhao, Z.-D. (2011). Fragments of hot and metasomatized mantle lithosphere in middle Miocene ultrapotassic lavas, southern Tibet. *Geology*, *39*, 923–926. https://doi.org/10.1130/G32172.1
Liu, M., & Yang, Y. (2003). Extensional collapse of the Tibetan plateau: Results of three-dimensional finite element modeling. *Journal of Geophysical Research*, *108*(B8), 2361. https://doi.org/10.1029/2002jb002248
Lowman, J. P., & Gable, C. (2008). Plumes anchored by a high viscosity lower mantle in a 3D mantle convection model featuring dynamically evolving plates. *Geophyiscal Research Letters*, *35*, L19309. https://doi.org/10.1029/2008GL035342
Maierová, P., Schulmann, K., Lexa, O., Guillot, S., Štipská, P., Janoušek, V., & Čadek, O. (2016). European Variscan orogenic evolution as an analogue of Tibetan-Himalayan orogen: Insights from petrology and numerical modeling. *Tectonics*, *35*, 1760–1780. https://doi.org/10.1002/2015TC004098
Mei, S., Bai, W., Hiraga, T., & Kohlstedt, D. L. (2002). Influence of melt on the creep behavior of olivine-basalt aggregates under hydrous conditions. *Earth and Planetary Science Letters*, *201*(3-4), 491–507. https://doi.org/10.1016/s0012-821x(02)00745-8
Mei, S., & Kohlstedt, D. L. (2000). Influence of water on plastic deformation of olivine aggregates: 1. Diffusion creep regime. *Journal of Geophysical Research*, *105*(B9), 21457–21469. https://doi.org/10.1029/2000JB900179
Meissner, R., & Mooney, W. (1998). Weakness of the lower continental crust: A condition for delamination, uplift, and escape. *Tectonophysics*, *296*(1-2), 47–60. https://doi.org/10.1016/s0040-1951(98)00136-x
Molina, J. F., Montero, P., Bea, F., & Scaroow, J. H. (2012). Anomalous xenocryst dispersion during tonalite-granodiorite crystal mush hybridization in the mid crust: Mineralogical and geochemical evidence from variscan appinites (avila batholith, central iberia). *Lithos*, *153*, 224–242. https://doi.org/10.1016/j.lithos.2012.03.021
Montel, J. M., Marignac, C., Barbey, P., & Pichavant, M. (1992). Thermobarometry and granite genesis: The hercynian low-P, high-T Velay anatectic dome (French massif central). *Journal of Metamorphic Geology*, *10*(1), 1–15. https://doi.org/10.1111/j.1525-1314.1992.tb00068.x
Montero, P., Bea, F., Zinger, T. F., Scarrow, J. H., Molina, J. F., & Whitehouse, M. (2004). 55 Million years of continuous anatexis in central Iberia: Single-zircon dating of the Peña Negra Complex. *Journal of the Geological Society*, *161*, 255–263. https://doi.org/10.1144/0016-764903-024
Moresi, L., & Gurnis, M. (1996). Constraints on the lateral strength of slabs from three-dimensional dynamic flow models. *Earth and Planetary Science Letters*, *138*(1-4), 15–28. https://doi.org/10.1016/0012-821x(95)00221-w
Mougeot, R., Respaut, J.-P., Ledru, P., & Marignac, C. (1996). U-Pb chronology on accessory minerals of the Velay anatectic dome (French massif central). *European Journal of Mineralogy*, *9*(1), 141–156. https://doi.org/10.1127/ejm/9/1/0141
Murphy, J. B. (2013). Appinite suites: A record of the role of water in the genesis, transport, emplacement and crystallization of magma. *Earth-Science Reviews*, *119*, 35–59. https://doi.org/10.1016/j.earscirev.2013.02.002
Nelson, K. D. (1992). Are crustal thickness variations in old mountain belts like the Appalachians a consequence of lithospheric delamination? *Geology*, *20*(6), 498. https://doi.org/10.1130/0091-7613(1992)020<0498:actvio>2.3.co;2
Nelson, K. D., Zhao, W., Brown, L. D., Kuo, J., Che, J., Liu, X., et al. (1996). Partially molten middle crust beneath southern Tibet: Synthesis of project INDEPTH results. *Science*, *274*(5293), 1684–1688. https://doi.org/10.1126/science.274.5293.1684
Petford, N., & Gallagher, K. (2001). Partial melting of mafic (amphibolitic) lower crust by periodic influx of basaltic magma. *Earth and Planetary Science Letters*, *193*(3-4), 483–499. https://doi.org/10.1016/s0012-821x(01)00481-2
Platt, J. P., & England, P. C. (1994). Convective removal of lithosphere beneath mountain belts: Thermal and mechanical consequences. *American Journal of Science*, *294*(3), 307–336. https://doi.org/10.2475/ajs.294.3.307
Prelević, D., Jacob, D. E., & Foley, S. F. (2013). Recycling plus: A new recipe for the formation of Alpine-Himalayan orogenic mantle lithosphere. *Earth and Planetary Science Letters*, *362*, 187–197. https://doi.org/10.1016/j.epsl.2012.11.035
Ranalli, G., & Murphy, D. C. (1987). Rheological stratification of the lithosphere. *Tectonophysics*, *132*(4), 281–295. https://doi.org/10.1016/0040-1951(87)90348-9
Rey, P. F., Teyssier, C., & Whitney, D. L. (2010). Limit of channel flow in orogenic plateaux. *Lithosphere*, *2*(5), 328–332. https://doi.org/10.1130/l114.1
Rosenberg, C. L., & Handy, M. R. (2005). Experimental deformation of partially melted granite revisited: Implications for the continental crust. *Journal of Metamorphic Geology*, *23*(1), 19–28. https://doi.org/10.1111/j.1525-1314.2005.00555.x
Rudnick, R. L., & Fountain, D. M. (1995). Nature and composition of the continental crust: A lower crustal perspective. *Reviews of Geophysics*, *33*(3), 267. https://doi.org/10.1029/95rg01302
Rybacki, E., Gottschalk, M., Wirth, R., & Dresen, G. (2006). Influence of water fugacity and activation volume on the flow properties of fine-grained anorthite aggregates. *Journal of Geophysical Research*, *111*, B03203. https://doi.org/10.1029/2005jb003663
Schilling, F. R., Partzsch, G. M., Brasse, H., & Schwarz, G. (1997). Partial melting below the magmatic arc in the central andes deduced from geoelectromagnetic field experiments and laboratory data. *Physics of the Earth and Planetary Interiors*, *103*(1-2), 17–31. https://doi.org/10.1016/s0031-9201(97)00011-3
Schutt, D. L., & Lesher, C. E. (2006). Effects of melt depletion on the density and seismic velocity of garnet and spinel lherzolite. *Journal of Geophysical Research*, *111*, B05401. https://doi.org/10.1029/2003jb002950
Sonder, L. J., & Jones, C. H. (1999). Western United States extension: How the west was widened. *Annual Review of Earth and Planetary Sciences*, *27*(1), 417–462. https://doi.org/10.1146/annurev.earth.27.1.417
Sylvester, P. J. (1998). Post-collisional strongly peraluminous granites. *Lithos*, *45*(1-4), 29–44. https://doi.org/10.1016/s0024-4937(98)00024-3
Teyssier, C., & Whitney, D. L. (2002). Gneiss domes and orogeny. *Geology*, *30*(12), 1139–1142.
Thompson, A. B., & Connolly, J. A. D. (1995). Melting of the continental crust: Some thermal and petrological constraints on anatexis in continental collision zones and other tectonic settings. *Journal of Geophysical Research*, *100*(B8), 15,565–15,579. https://doi.org/10.1029/95jb00191
Turner, S., Arnaud, N., Liu, J., Rogers, N., Hawkesworth, C., Harris, N., et al. (1996). Post-collision, shoshonitic volcanism on the Tibetan Plateau: Implications for convective thinning of the lithosphere and the source of ocean island basalts. *Journal of Petrology*, *37*(1), 45–71. https://doi.org/10.1093/petrology/37.1.45
Ueda, K., Gerya, T. V., & Burg, J.-P. (2012). Delamination in collisional orogens: Thermomechanical modeling. *Journal of Geophysical Research*, *117*, B08202. https://doi.org/10.1029/2012jb009144
Väisänen, M., Mänttäri, I., Kriegsman, L. M., & Hölttä, P. (2000). Tectonic setting of post-collisional magmatism in the palaeoproterozoic Svecofennian orogen, SW Finland. *Lithos*, *54*(1-2), 63–81. https://doi.org/10.1016/s0024-4937(00)00018-9
van Hunen, J., Zhong, S., Shapiro, N. M., & Ritzwoller, M. H. (2005). New evidence for dislocation creep from 3-D geodynamic modeling of the Pacific upper mantle structure. *Earth and Planetary Science Letters*, *238*(1-2), 146–155. https://doi.org/10.1016/j.epsl.2005.07.006
Vanderhaeghe, O., & Teyssier, C. (2001). Crustal-scale rheological transitions during late-orogenic collapse. *Tectonophysics*, *335*(1), 211–228.

Vigneresse, J. L., Barbey, P., & Cuney, M. (1996). Rheological transitions during partial melting and crystallization with application to felsic magma segregation and transfer. *Journal of Petrology*, *37*(6), 1579–1600. https://doi.org/10.1093/petrology/37.6.1579

Wang, Y., Zhang, J., Jin, Z., & Green, H. (2012). Mafic granulite rheology: Implications for a weak continental lower crust. *Earth and Planetary Science Letters*, *353*, 99–107.

Wei, C., & Powell, R. (2003). Phase relations in high-pressure metapelites in the system KFMASH (K_2O-FeO-MgO-Al_2O_3-SiO_2-H_2O) with application to natural rocks. *Contributions to Mineralogy and Petrology*, *145*(3), 301–315. https://doi.org/10.1007/s00410-003-0454-1

White, R. W., Powell, R., & Holland, T. J. B. (2001). Calculation of partial melting equilibria in the system Na_2O-CaO-K_2O-FeO-MgO-Al_2O_3-SiO_2-H_2O (NCKFMASH). *Journal of Metamorphic Geology*, *19*(2), 139–153. https://doi.org/10.1046/j.0263-4929.2000.00303.x

White, R. W., Powell, R., & Phillips, G. N. (2003). A mineral equilibria study of the hydrothermal alteration in mafic greenschist facies rocks at kalgoorlie, Western Australia. *Journal of Metamorphic Geology*, *21*(5), 455–468. https://doi.org/10.1046/j.1525-1314.2003.00454.x

Williamson, B. J., Downes, H., & Thirlwall, M. F. (1992). The relationship between crustal magmatic underplating and granite genesis: An example from the velay granite complex, massif central, France. *Transactions of the Royal Society of Edinburgh: Earth Sciences*, *83*(1-2), 235–245. https://doi.org/10.1017/s0263593300007926

Yuen, D. A., & Fleitout, L. (1985). Thinning of the lithosphere by small-scale convective destabilization. *Nature*, *313*(5998), 125–128. https://doi.org/10.1038/313125a0

Zhong, S., Zuber, M. T., Moresi, L., & Gurnis, M. (2000). Role of temperature-dependent viscosity and surface plates in spherical shell models of mantle convection. *Journal of Geophysical Research*, *105*(B5), 11,063–11,082.